UCRL-JRNL-207219

A Unified Model of Secondary Electron Cascades in Diamond

B. Ziaja, R. A. London, J. Hajdu

October 14, 2004

Journal of Applied Physics

PACS Classification: $79.20.Hx, 82.53.Ps, 61.80.-x$

A UNIFIED MODEL OF SECONDARY ELECTRON CASCADES IN DIAMOND

Beata Ziaja [*,†], Richard A. London [§], Janos Hajdu [*] [1]

[*] *ICM Molecular Biophysics, Biomedical Centre, Uppsala University, Husargatan 3, Box 596, S-75123 Uppsala, Sweden*

[†] *Department of Theoretical Physics, Institute of Nuclear Physics, Radzikowskiego 152, 31-342 Cracow, Poland*

[§] *Lawrence Livermore National Laboratory, Livermore, CA 94551, USA*

[1] e-mail:ziaja@tsl.uu.se, , rlondon@llnl.gov, hajdu@xray.bmc.uu.se

Abstract:

In this paper we present a detailed and unified theoretical treatment of secondary electron cascades that follow the absorption of an X-ray photon. A Monte Carlo model has been constructed that treats in detail the evolution of electron cascades induced by photoelectrons and by Auger electrons following inner shell ionizations. Detailed calculations are presented for cascades initiated by electron energies between $0.1 - 10$ keV. The present paper expands our earlier work [1,2] by extending the primary energy range, by improving the treatment of secondary electrons, especially at low electron energies, by including ionization by holes, and by taking into account their coupling to the crystal lattice. The calculations describe the three-dimensional evolution of the electron cloud, and monitor the equivalent instantaneous temperature of the free-electron gas as the system cools. The dissipation of the impact energy proceeds predominantly through the production of secondary electrons whose energies are comparable to the binding energies of the valence ($40 - 50$ eV) and of the core electrons (300 eV). The electron cloud generated by a 10 keV electron is strongly anisotropic in the early phases of the cascade ($t \leq 1$ fs). At later times, the sample is dominated by low energy electrons, and these are scattered more isotropically by atoms in the sample. Our results for the total late time number of secondary electrons agree with available experimental data, and show that the emission of secondary electrons approaches saturation within about 100 fs, following the primary impact.

Introduction

The damage to solid materials caused by X-ray irradiation is of interest to several research disciplines. Radiation damage is the limiting factor in the achievable resolution for biological materials in X-ray diffraction as well as in electron microscopy [3–5]. New, X-ray sources, like free electron lasers (XFELs) will soon provide very short, intense pulses that may allow existing damage limitations to be overcome [6]. A fundamental understanding of the interaction of X-rays with solid state materials is important to pursue this possibility. Damage is also a limiting factor in the design of X-ray optics [7] and detectors for XFELs and for the survival of samples exposed to their intense X-ray beam. On the positive side, production of "warm dense matter" [8] by XFELs will be mediated by those same electron cascades that underlie the damage processes. Also, interpretation of recent experiments on non-thermal melting in solids [9] and some unexpected behavior of xenon clusters exposed to very short X-ray pulses [10] depend on an understanding of electron cascades.

X-rays interact with the material mainly via the photoelectric effect. In light elements, the emission of an energetic photoelectron is followed by the emission of a less energetic Auger electron [6]. These electrons propagate through the sample, and cause further damage by excitations of secondary electrons. The extent of ionisation will depend on the size of the sample. Photoelectrons released by X-rays of ~ 1 Å wavelength are fast, $v \sim 660$ Å/fs, and they can escape from small samples early in an exposure. In contrast, Auger electrons are slow ($v \sim 95$ Å/fs in carbon), so they remain longer in a sample, and it is likely that they will thermalize there. A detailed description of electron cascades initiated by an electron impact of energy between $\sim 0.1 - 10$ keV is needed for a better understanding of radiation damage

in larger samples as secondary ionization caused by propagating photoelectrons becomes significant there.

Electron transport in different materials and the related phenomena: energy deposition and impact ionization have been extensively studied [11–35]. These studies have been restricted to: (i) higher electron impact energies, $E > 100$ eV (see e.g. [23–26]), following slowing down of an energetic primary electron, or to (ii) the very low energies, $E < 10$ eV, as needed for describing the transport of hot carriers in semiconductors (see e.g. [29–35]). The novelty of our approach is to unify these two descriptions and to implement them into one simple model. This model is aimed at accurately calculating the space and time dependence of the impact ionization in diamond resulting from the slowing down a photoelectron or an Auger electron.

The present analysis extends our previous studies [1,2,7]. The model of [7] did not include time dependence and lacked a detailed treatment of the spatial transport of low energy electrons ($E < 1$ keV). In the subsequent time-dependent studies on the electron transport in diamond [1,2], we neglected the possible impact ionizations by holes and did not treat the electron coupling to the crystal lattice mediated by phonons.

The time dependence is particularly important in understanding whether the performance of an optical component will be altered during an XFEL pulse, typically 20 to 300 fs in duration. The performance of certain optics, such as X-ray diffraction crystals, will be altered if the X-ray energy is coupled into lattice motion during the pulse. A crucial step in this coupling is the electron cascade from the initial X-ray absorption event down to low energy electrons (typically $5 - 20$ eV), which then couple to the lattice. This coupling can be both by thermal (electron-lattice collisions) and non-thermal (electrostatic) mechanisms. The

treatment of holes is important since they significantly add to the total number of ionizations.

Here, we present results from the extended Monte Carlo simulations, showing the detailed space-time evolution of secondary electron cascades in a diamond crystal over a significantly extended primary energy range. The model treats both the impact ionization by secondary electrons and holes down to the very low impact energies of the carriers, and the coupling of the carriers to the crystal lattice. The accuracy of our model should be sufficient for estimating the impact ionization rate by electrons and holes as needed in the simulations of the sample irradiated by photons from the FEL. Although the electron transport in solids has been extensively studied using different techniques, up to our knowledge, no time resolved analysis of the impact ionization by electrons in diamond, directly applicable for the FEL studies, have been yet published.

Model

Calculations of electron trajectories

Electrons moving inside a solid interact with the atoms of the solid. If the kinetic energy of the electrons is high, they propagate almost freely through the sample, and collide with single atoms [36,37]. This interaction may be either elastic or inelastic. Electrons also interact with the crystal lattice, emitting (and absorbing) phonons. These interactions may be neglected at high energies. Inelastic scattering usually results in impact ionization followed by the release of an electron-hole pair in semiconductors and insulators. Simple scaling considerations predict that if valence electrons are ionized, their kinetic energies should not be much larger

than a few times the shell binding energy. At higher impact energies the core electrons may also be ionized. Using cross sections described below, Figure 1 shows that the mean energy of the secondary electrons in diamond is about $40 - 60$ eV (close to the energy of L shell electrons), reaching peak energies of about 300 eV (close to the energy of core electrons). The energy loss, ω, does not exceed 300 eV (at the 95% probability level), and its value becomes independent of the impact energy, E, at energies greater than 1 keV. This can be expected as one-electron excitations are predominant in inelastic scattering [38,39].

When the incoming electron is fast, we can use the Bethe-Fermi approximation [38,39]. It replaces the electric field of the incoming electron by an electromagnetic pulse of the same, short duration. Impact ionization is then proportional to the dipole transition probability caused by the short, non-periodic electromagnetic pulse. The Bethe-Fermi approximation is the basis of the optical model that we use below.

The primary (impact) electron loses its energy in a secondary electron cascade. When reaching an energy of $200-300$ eV, the electron de Broglie wavelength becomes comparable with the atomic separation. At lower energies the electron interacts multiply with a cluster of neighbouring atoms, the size of which is of the order of the de Broglie wavelength [40]. For such low energies the Born approximation is not valid, and including a non-local exchange and correlation term into the interaction potential becomes necessary for an accurate description of electron scattering [15]. At the same time the electron-phonon coupling increases although it is still small compared to the electron-atom elastic cross section [33].

In this paper, as in the previous studies [1,2], we use the formalism of the Lindhard dielectric function [41] with the TPP-2 optical model [14,16,22] for the description of the inelastic

interactions of electrons with atoms of the sample. This approach is based on the Bethe-Fermi approximation, and it takes into account both valence and core ionizations of the atoms in a solid, where the cross section for core ionizations is not higher than about 10 % of the total ionization cross section in the solid [42]. We use this model as it accurately provides the electron inelastic cross sections in solids over a wide energy range, $0.05 < E < 10$ keV, particularly at lower energies ($E < 200 - 300$ eV), where the atomic models fail.

At low energies ($E < 50$ eV) inelastic cross sections calculated with the optical models cannot be fully trusted [15]. Exchange and correlation terms in the atomic potential, and the complex structure of the energy band strongly influence the dynamics of the scattered electrons, and an accurate calculation of the impact ionization rate should include these effects. The first-principles calculations are then required in order to estimate the ionization rate by electrons and holes. For diamond such calculations were performed by Watanabe et al. [43] at very low impact energies. In this approach the band structure was calculated using the empirical pseudopotential method, and the dielectric function was evaluated with the calculated band structure. Fig. 2 shows the inelastic mean free path obtained with Watanabe's model for impact ionization of diamond at very low energies ($E < 20$ eV). This mean free path was calculated, including the three lowest conduction bands and three highest valence bands.

At the intermediate energies ($20 < E < 50$ eV) both Watanabe's and the TPP-2 models are beyond their validity region. However, no other models are known to describe the inelastic scattering of electrons accurately at those energies. Therefore we extrapolate both Watanabe's and the TPP-2 models to the intermediate energies, and then compare the accuracy of their predictions at this energy regime.

Fig. 2 shows the striking difference between the low- and the high energy approaches. At energies $E > 10$ eV the Watanabe's mean free path decreases more rapidly than the TPP-2 mean free path (extended to energies below 50 eV), reaching unrealistically low values already at $E = 20$ eV. It seems that using only the partial band structure (the three lowest conduction bands and three highest valence bands) restricts the validity of Watanabe's results to even to lower impact energies, $E \leq 10$ eV.

At lower energies of about $9 - 10$ eV both the TPP-2 and Watanabe's mean free paths overlap, and the Watanabe mean free path path extends further down to the impact threshold energy, $E_{gap} = 5.47$ eV. The TPP-2 mean free path cannot be calculated at energies lower than 9 eV, due to the low accuracy of the data on the optical loss function in this energy region. In our previous publications [1,2] we assumed that there is no impact ionization possible for impact electrons below these energies within the TPP-2 model.

Therefore it seems natural to use the Watanabe's results that are valid at very low energies [43] in order to extrapolate the inelastic mean free path obtained with the extended TPP-2 model ($9 < E < 50$ eV) to energies lower than 9 eV. The unified model obtained will be called the WTPP-2 model. We tested the accuracy of this approximation performing a set of the dedicated Monte-Carlo simulations. The results of this test will be discussed later.

The Ashley's mean free path is much larger than Watanabe's inelastic mean free path at low energies, therefore we will not use Ashley's model in the forthcoming analysis.

As in previous studies, we treat elastic scattering of the incoming electron with atoms in the muffin-tin potential approximation [1,2,36,37]. To estimate the elastic scattering of low-energy electrons ($E < 0.4$ keV), we use programs from the Barbieri/Van Hove Phase Shift

package [44]. For $E \geq 0.4$ keV we obtain elastic cross sections from the NIST database [28]. Fig. 3 shows the total elastic and inelastic cross sections obtained from the calculations. The results show that for energies higher than 1 keV, the elastic and inelastic cross sections are comparable, but for lower energies, $0.1 < E < 1$ keV, the elastic cross section is twice as large as the inelastic one. For very low energies, $E < 0.1$ keV, the inelastic cross sections drop rapidly, and elastic interactions become predominant. The electron-phonon coupling becomes significant for carriers of very low impact energies, $E < E_{gap}$ [33–35, 45].

Core ionization

Fig. 4 shows the energy loss function (ELF) and the cross sections for core ionization from the K shell of carbon as estimated from the Lindhard approximation, using the optical models. The energy loss function is the sum of the large valence and small core contributions. We make a rough estimate of the pure core contribution by subtracting the valence component from the ELF. The valence component was extrapolated above the core ionization edge (cf. Fig. 4).

The cross sections in Fig. 4b are compared to results from the recent version of the binary- encounter-Bethe model (RBEB) [46] for the total core ionization by impact electrons. This model was developed by combining a modified form of the Mott cross section and the leading dipole part of the Bethe cross section [47].

The cross section obtained from our estimate is smaller than the RBEB cross section at energies smaller than $1 - 2$ keV. At larger energies our estimate agrees well with the RBEB predictions. The discrepancy at lower energies (Fig. 4b) is due to two factors that: (i) it is difficult to separate the contribution of the core excitations from the valence excitations

on the basis of the ELF alone, and (ii) the optical approximation does not apply at the core excitation threshold. However, this does not affect our results significantly, since we do not need to make any separation between the valence and the core ionizations, and valence ionizations dominate. Therefore, the potential errors resulting from the separation will not affect the final results.

Holes

Impact ionization of a valence electron in a semiconductor or insulator always releases a pair of carriers: an electron and a hole. When far from the solid surface, the holes behave as free carriers moving inside the valence band. The relation between the energy and the momentum of the hole is described by a dispersion relation depending on the band structure. The holes may cause further impact ionizations, and the respective ionization cross sections can be estimated from first-principles calculations with the band structure [30–32,48,49]. The results obtained for several semiconductors [35] show that these cross sections are comparable to the cross sections for ionization by impact electrons. This approach may be also applied for diamond where the effective mass of a hole is similar to the mass of a free electron [50]. Therefore we use the electronic impact cross sections as a first approximation for the ionization cross sections by hole impact.

Impact ionization at very low energies

In semiconductors, the rate of impact ionization at low energies based on first-principles calculation can be fitted as, $\Gamma = a(E - E_{th})^b$, where a and b are coefficients specific for the semiconductor, and the threshold energy, $E_{th} \geq E_{gap}$ [30–32,49]. Coefficients a and b are calculated so as to get Γ in [1/fs] units with energy expressed in [eV] units. We fitted this

relation to the ionization rate obtained by Watanabe et al. [43] for diamond with $a = 5.53 \cdot 10^{-5}$, $b = 4.33$ and hence obtained the respective mean free path, $\lambda = v_{e,h}/\Gamma$, where $v_{e,h}$ denoted the velocity of the carrier. The energy of the primary electron after ionization and the energies of secondaries were obtained within the random-k approximation [29,51]. In this approximation the energies of the secondary electron, the hole, and of the primary electron are proportional to their respective densities of states, derived from the density of states of the valence and the conduction band respectively, $\rho_{V,C}(E)$ [51],

$$P(E_h|E) = \frac{\rho_V(E_h) \int dE_e \, \rho_C(E - E_h - E_e - E_{gap}) \, \rho_C(E_e)}{\int dE_h \, \rho_V(E_h) \int dE_e \, \rho_C(E - E_h - E_e - E_{gap}) \, \rho_C(E_e)} \quad (1)$$

$$P(E_e|E, E_h) = \frac{\rho_C(E_e) \, \rho_C(E - E_h - E_e - E_{gap})}{\int dE_e \, \rho_C(E_e) \, \rho_C(E - E_h - E_e - E_{gap}).} \quad (2)$$

Here P denotes conditional probabilities to produce a hole of energy, E_h, and an electron of energy, E_e, from a primary electron of energy, E. A similar relation can be written to describe the ionization by the impact of holes.

Band structure

Calculating the conditional probabilites, we used the densities of states of the valence and the conduction bands obtained from the band structure calculations of Barnard, Russo and Snook [52]. The calculations were performed for crystal diamond. The (unnormalized) densities of states were evaluated with the CRYSTAL98 code for both the valence and the conduction band. Fig. 5 shows the results.

Momentum conservation

After impact ionization at high impact energies the differential cross sections determine the energy loss of the primary electron and its scattering angle. At low impact energies we obtain the energies of all carriers: the primary electron and the secondary electron and the

hole with the random-k approximation [29,51]. The scattering angle of the primary carrier is then chosen randomly. The energies of carriers are proportional to the density of states of the valence band in which they are created. The energies of the primary and secondary carriers determine the magnitude of their momenta, following the dispersion relations in the respective bands. Here we assume the quadratic dispersion relation for both electrons and holes [40].

The momentum transfer, $\mathbf{\Delta k} = \mathbf{k}'_i - \mathbf{k}_i$, is then estimated from the scattering angle of the primary carrier, and the momentum conservation for the production of an electron-hole pair by a carrier impact requires,

$$\mathbf{k}'_e + \mathbf{k}'_h = -\mathbf{\Delta k} \tag{3}$$

where $\mathbf{k}'_e, \mathbf{k}'_h$ denote the momenta of the electron and hole released.

Phonons

The accurate calculation of the carrier-phonon scattering in a semiconductor requires complicated first-principles calculations including the band structure [35]. However, the energy gains or losses due to phonons are small, $E < 0.1$ eV, and do not influence significantly the dynamics of impact ionization. Since we are primarily interested in processes that contribute significantly to the impact ionization rate, we do not take these gains and losses into account.

The carrier-phonon scatterings that occur mostly at low energies will then only lower the ionization rate of the sample. Therefore, we do not require high accuracy in the description of the phonon coupling, and we describe this coupling in our cascade model using a simple fit. We assume that at very low energies the carrier-phonon total scattering rate is proportional to the density of states, $\sim \rho_{V(C)}(E)$ [30,53], and that at higher energies this rate decreases

as $\sim 1/\sqrt{E}$ [33]. These two approximations are linked at the energy of about 5 eV which corresponds to the deformation potential constant calculated for acoustic phonon in diamond [54]. The total scattering rate thus obtained was used to estimate the mean free paths for the electron- and the hole-phonon scattering in diamond. However, possible gains and losses of carrier energy ocurring in these scatterings are neglected in the simulations.

Results on impact ionization by electrons and holes

Using the model described above, we performed a set of Monte Carlo simulations to follow the path of impact electron and the secondary electrons and holes in diamond. We use a coordinate system with the starting position of the impact electron at $t = 0$ at the origin, and the velocity of the impact electron along the Z-axis. The space-time characteristics of secondary cascades of electrons and holes were recorded as a function of the impact energy.

Evolution of each cascade was analysed through the number of secondary electrons, $N_{el}(t)$, and the equivalent temperature of the free electron gas $kT(t) = 2/3 \cdot E/N$, where E is the total kinetic energy of electrons, and $N = N_{el} + 1$ is the total number of electrons. We use this definition because, although the electron gas is far from thermal equilibrium, the equivalent temperature is still a quantity conserved in electron-electron collisions. These quantities were averaged over 200 cascades. Figures 6, 7 show the results obtained with the TPP-2 optical model and the WTPP-2 model for impact energies of $E = 0.1, 0.25, 1, 10$ keV.

The number of electrons emitted increased in time, and saturated within $10 - 100$ fs with a total of about 8,20,80 and 800 electrons released at impact energies of $E = 0.1, 0.25, 1, 10$

keV respectively.

In the context of nuclear radiation detectors, several experimental studies have found an average pair creation energy by high energy electrons and ions in diamond between 12.8 and 13.6 eV [55–57] with 13 eV being the most recent result [57]. Previous theoretical work on cascades initiated by electrons suggests pair creation values between 10.3 and 11.6 eV [58,59]. Experimental values for the pair creation energy agree well with the values found in our simulations, 12.5 eV with the TPP-2 model, and 12 eV with the WTPP-2 model. For example, using 13 eV as the average pair creation energy, one would predict about 770 ionizations for a 10 keV electron, compared to values of 800 and 830 obtained with the TPP-2 and WTPP-2 models respectively.

The data on the pair creation energy enable also checking the accuracy of the WTPP-2 model and the TPP-2 model at low energies. As the cross sections obtained from the TPP-2 model may be not reliable below 50 eV, we have investigated how the number of ionizations changes if we do not use the TPP-2 model at low energies, and apply instead another model, e. g. adapted RBEB model, to link the mean free path with the TPP-2 model (at high energies) to the Watanabe's model (at very low energies). Using this approach, the average energy for the creation of an electron-hole pair estimated from the number of secondaries was about 9.8 eV. This is below the previous theoretical predictions [58,59], and much below experimental results [55–57]. Therefore the TPP-2 and WTPP-2 model seem to be appropriate to describe these very low energy electron cascades in diamond. The small difference in the number of ionization events obtained with these two models is due to the fact that the WTPP-2 model allows ionizations by impacts of very low energies ($E < 9$ eV) whereas the

pure TPP-2 model does not allow this.

In [2] we estimated the total number of ionization events triggered by an electron impact of energy, $E = 0.25$ keV to be, $N_{el} = 13$, at 90 fs. In this paper we obtain about 20 ionization events at the same value of the electron impact. The increase is due to the neglect of ionization by holes in our previous studies.

While simulating the cascades of secondary electrons and holes initiated by single electron impacts, we used the elastic and inelastic cross sections calculated for a sample of neutral atoms. That was a good approximation as in that case the fraction of ionized atoms in the sample was small. If carrier cascades are initiated by many impact electrons simultaneously, the fraction of ions in the sample becomes large, and the approximation of a neutral medium breaks down. However, the cross sections for the impact ionization of the ions are much smaller than the cross sections for the impact ionization of neutral atoms. Therefore our results obtained within the neutral medium approximation represent the upper limit of the number of possible impact ionizations ocurring in a real case, when a fraction of atoms has been ionized.

The equivalent temperature of the electron gas (calculated including the primary electron) decreased as the cascade evolved (Fig. 7a). We note that after about 10 fs, all temperature curves showed similar overall features, and these were independent from the energy of the primary impact particle. This indicated that the average energy of electrons was not much influenced by the energy of the primary electron but rather by secondary electrons of lower energies (< 60 eV) which dominated the sample after 10 fs. At 100 fs the temperature of the electron gas dropped to $\sim 2 - 2.2$ eV. In a similar way we estimate also the equivalent

temperature of the secondary electrons and holes shown in Figs. 7b-c. The results show similar curve shapes for secondary electrons and holes. The temperature of the carrier gas increased to a peak value within ~ 0.1 fs (electrons) and ~ 1 fs (holes), and then decreased, reaching (at ~ 10 fs) a final temperature independent of the primary impact energy.

Figs. 8a shows plots of the average number of electrons released, N_{el}; (b-c) the equivalent temperature, kT, of the electron gas as a function of the energy, E, of the primary electron at different times. These curves describe results obtained at $1, 10, 90$ fs, and were based on the TPP-2 model and the WTPP-2 model. The data represent primary energies of $E = 0.1, 0.25, 1, 10$ keV. The results can be used for the interpolation of the number of ionizations, and the temperature of the electrons at energies ranging from $E = 0.1$ keV to $E = 10$ keV. The results show that the number of secondary electrons, N_{el}, is proportional to the impact energy.

The energy distribution of secondary electrons. The positions and velocities of electrons recorded at times, $t = 1$, 10, 90 fs at energies of $E = 0.1, 0.25, 1, 10$ keV were collected from all cascades, and put into one file. Using these data, histograms for the energy distributions were obtained, $N(E)/N$, at these time points. Number, $N(E) = \sum_{i=1}^{200} N_i(E)$, is the total number of electrons in a bin, $(E, E + \Delta E)$, obtained from summing up the results, $N_i(E)$, from all cascades. Correspondingly, $N_i(E)$ is the number of electrons found in that bin for the ith cascade. These distributions were normalized to the total number of electrons, $N = \sum_E N(E)$. Fig. 9 shows the histograms at impact energies of $E = 0.1$ keV and $E = 10$ keV. As expected, the energy histograms show that the number of low-energy electrons increased with time. One may notice that the dissipation of the impact energy is fast. Both the

TPP-2 and the WTPP-2 models predict that at $t = 1$ fs after the primary emission most of the electrons will have energy lower than 60 eV, independently of the energy of the primary impact. Similarly, at 10 fs the energy of the most of the electrons will be lower than 25 eV, and at 90 fs lower than 12 eV.

The plots show the characteristic and well-known shape of the secondary electron (hole) distributions [23,24]: the distribution rapidly increases at very low energies reaching a peak value at a few electronovolts, and then smoothly decreases, forming a long tail extending to high energies. The position of the peak moves towards lower energies, as the number od secondary electrons increases. The peak is located at ~ 5 eV after 10 fs from the primary electron emission, and at ~ 2 eV after 100 fs. The distributions of hole energies show a similar tendency. The histograms for electrons and holes become comparable at $t = 90$ fs after the primary electron emission, when the impact energy has already dissipated.

Spatial distribution of secondary electrons. In order to describe the spatial distribution of the secondary electron cloud in cascades triggered by $E = 0.1$ and $E = 10$ keV electrons, results from all simulations were analysed at these energies. Fig. 10 shows the local normalized density of electrons and holes from the TPP-2 model at times, $t = 1, 10, 90$ fs created by single electron impacts with velocity along the Z-axis. The normalization condition requires, $\sum_i \rho_i V_i = 1$, where ρ_i is the carrier density measured in the volume, V_i. The (normalized) density of electrons is distributed on the $r_{xy} = \sqrt{x^2 + y^2}$ and z plane and localized around the position of the primary impact. At longer time scales, $t > 10$ fs, the density becomes smoother, and this peak becomes smaller. At 90 fs the electron cloud spreads to $(R_{xy}, Z_-, Z_+) = (60, -100, 70)$ Angstroms and $(R_{xy}, Z_-, Z_+) =$

$(200, -200, 800)$ Angstroms at energies $E = 0.1$ and 10 keV. Results from the WTPP-2 model were very similar and are not shown separately.

Conclusions

A simple model was constructed in order to describe the dynamics of the impact ionizations released by an electron or a hole impact in diamond. The model joins together a Bethe-Fermi treatment using optical model approach at high energies with a band structure model at low energies. Impact ionization by holes is included. The results obtained have been used to estimate ionization by electrons of different impact energies ($E = 0.1 - 10$ keV) in diamond. The main results are: (i) 8-800 secondary electrons released at different impact energies $E = 0.1 - 10$ keV. These numbers are in agreement with previous experiments and calculations, (ii) time dependent results, showing that the typical cascade time ranges from 10 fs to 100 fs at $E = 0.1 - 10$ keV. The spatial extent of the electron cloud ranges from $(R_{xy}, Z_-, Z_+) = (60, -100, 70)$ Angstroms at $E = 10$ keV to $(R_{xy}, Z_-, Z_+) = (200, -200, 800)$ Angstroms at $E = 10$ keV. The energy distribution is asymmetric. It peaks at low energies and then smoothly decreases forming a tail at higher energies.

The Monte-Carlo code may be adapted to simulate ionization phenomena in different systems, ranging from the explosion of atomic clusters to the formation of warm dense matter and plasmas. The model can also be used to estimate ionization rates and the spatio-temporal characteristics of secondary electron cascades in biological substances.

For 10 keV X-rays as to be generated by XFELs, the electron cascade will develop within

100 fs after the primary photoelectron emission. This time scale is comparable to the pulse length of these systems. Therefore the dynamics of the electron cascade may be quite important in the interaction of XFEL beams with materials such as diamond. It may be possible to study the time dependent electron cascades, as we have modelled, with a XFELs.

Acknowledgments

We are grateful to Abraham Szöke, Gyula Faigel, Zoltan Jurek, David van der Spoel and Michel A. van Hove for discussions. B. Z. thanks Peter Druck and the Institute of Theoretical Physics II at the Ruhr University in Bochum for providing access to the computational unit. This research was supported in part by the Polish Committee for Scientific Research with grant No. 2 P03B 05119, the EU-BIOTECH Programme and the Swedish Research Councils. B. Z. is a fellow of the Alexander von Humboldt Foundation. The work of R. L. was performed under the auspices of the Department of Energy by the University of California, Lawrence Livermore National Laboratory under contract No. W-7405-Eng-48.

References

[1] Ziaja, B., van der Spoel, D., Szöke, A., and Hajdu, J. *Phys. Rev. B* **64**, 214104 (2001).

[2] Ziaja, B., Szöke, A., van der Spoel, D., and Hajdu, J. *Phys. Rev. B* **66**, 024116 (2002).

[3] Henderson, R. *Proc. R. Soc. Lond. Biol. Sci.* **241**, 6–8 (1990).

[4] Henderson, R. *Q. Rev. Biophys.* **28**, 171–193 (1995).

[5] Sayre, D. and Chapman, H. N. *Acta Cryst. A* **51**, 237 (1995).

[6] Neutze, R., Wouts, R., van der Spoel, D., Weckert, E., and Hajdu, J. *Nature* **406**, 752–757 (2000).

[7] London, R. A., Bionta, R. M., Tatchyn, R. O., and Roesler, S. Optics for Fourth-Generation X-Ray Sources. *Proc. SPIE* **4500**, 51 (2001).

[8] Lee, R. W. et al. *Laser and Particle Beams* **20**, 527 (2002).

[9] Sokolowski-Tinten, K. and von der Linde, D. *Phys. Rev. B.* **61**, 2643 (2000).

[10] Wabnitz, H. et al. *Nature* **420**, 482 (2002).

[11] Peterson, L. R. *Phys. Rev.* **187**, 105 (1969).

[12] Inokuti, M. et al. *Phys. Rev. A* **38**, 1217 (1988).

[13] Powell, C. *J. Elec. Spec. Rel. Phenom.* **47**, 197 (1988).

[14] Tanuma, S., Powell, C., and Penn, D. *Surf. Interf. Anal.* **11**, 577 (1988).

[15] Tanuma, S., Powell, C., and Penn, D. *Surf. Interf. Anal.* **17**, 911 (1991).

[16] Tanuma, S., Powell, C. J., and Penn, D. R. *Surf. Interf. Anal.* **17**, 911 (1991).

[17] Ashley, J. *J. Elec. Spec. Rel. Phenom.* **46**, 199 (1988).

[18] Abril, I. et al. *Phys. Rev. A* **58**, 357 (1998).

[19] Penn, D. *Phys. Rev. B* **13**, 5248 (1976).

[20] Ashley, J. *J. Elec. Spec. Rel. Phenom.* **50**, 323–334 (1990).

[21] Ashley, J. *J. Appl. Phys.* **69**, 674 (1991).

[22] S. Tanuma, S. Ichimura, K. Y. *Appl. Surf. Scien.* **100/101**, 47 (1996).

[23] K. Nishimura, J. Kawata, K. O. *Nucl. Inst. Meth. Phys. Res. B* **164-165**, 903 (2000).

[24] Kuhr, J.-C. and Fitting, H.-J. *J. Elec. Spec. Rel. Phenom.* **105**, 257–273 (1999).

[25] Baró, J., Sempau, J., Fernández-Varea, J., and Salvat, F. *Nucl. Inst. Meth. Phys. Res. B* **100**, 31–46 (1995).

[26] Fernández-Varea, J. et al. *Nucl. Inst. Meth. Phys. Res. B* **108**, 35–50 (1996).

[27] Öztürk, N. and W. Williamson, J. *74* **J. Appl. Phys.**, 4723–4728 (1993).

[28] Jablonski, A. and Powell, C. **NIST Standard Reference Database**.

[29] Kane, E. O. *Phys. Rev.* **159**, 624 (1967).

[30] Jung, H. K., Taniguchi, K., and Hamaguchi, C. *J. Appl. Phys.* **79**, 2473 (1995).

[31] Kunikiyo, T. et al. *J. Appl. Phys.* **79**, 7718 (1996).

[32] Reigrotzki, M. et al. *J. Appl. Phys.* **86**, 4458 (1999).

[33] Arnold, D., Cartier, E., and DiMaria, D. *Phys. Rev. B* **49**, 10278 (1994).

[34] Fischetti, M. and Laux, S. *Proceedings of the 26th European Solid State Device Research Conference, Editions Frontieres* , 813 (1996).

[35] IBM Research. Damocles home page. *http://www.research.ibm.com/DAMOCLES* .

[36] Bransden, B. and Joachain, C. Physics of atoms and molecules. *Longman, Essex* , 505–513 (1998).

[37] Burke, P. Atomic, molecular and optical physics handbook. Editor G.W.F. Drake. *Woodbury, New York American Institute of Physics* , 536 (1996).

[38] Fermi, E. *Z. Phys.* **29**, 315 (1924).

[39] Bethe, H. *Ann. Phys. (Leipzig)* **5**, 325 (1930).

[40] Ashcroft, N. and Mermin, N. Solid state physics. *Harcourt, Inc.* (1976).

[41] Lindhard, J. *K. Dan. Vidensk. Selsk. Mat. Fys. Medd.* **28**, 1–57 (1954).

[42] Pianetta, P. *X-ray data booklet* , 3–5 (2001).

[43] Watanabe, T. et al. *Jpn. J. Appl. Phys. 2* **40(7B)**, L715 (2001).

[44] Barbieri, A. and van Hove, M. private communication; Phase Shift package, http://electron.lbl.gov/leedpack/. .

[45] Yoder, P. D. and Hess, K. *Semicon. Sci. Technol.* **9**, 852 (1994).

[46] Kim, Y.-K., Santos, J., and Parente, F. *Phys. Rev. A* **62**, 052710 (2000).

[47] Kim, Y.-K. and Rudd, M. *Phys. Rev. A* **50**, 3954 (1994).

[48] Gautam, D. K., Khokle, W. S., and Garg, K. B. *Phys. Stat. Sol.(b)* **145**, 269 (1988).

[49] Lorenzini, M. and van Houdt, J. *Solid-State Electron.* **46**, 223 (2002).

[50] Database on Semiconductors, http://www.ioffe.rssi.ru/SVA/NSM/Semicond/. .

[51] Kamakura, Y. et al. J. Appl. Phys. **88**, 5802 (2000).

[52] Barnard, A. S., Russo, S. P., and Snook, I. K. *Phil. Mag. B* **82**, 1767 (2002).

[53] Chen, Y. and Tang, T. *J. Appl. Phys.* **65**, 4279 (1989).

[54] Gamal, S. H. and Al-Harbi, T. *Microelec. J.* **32**, 327 (2001).

[55] Kozlov, S. F., Stuck, R., Hage-Ali, M., and Siffert, P. *IEEE Trans. Nucl. Sci* **NS-22**, 160 (1975).

[56] Canali, C. et al. *Nucl. Inst. Meth.* **160**, 73 (1979).

[57] Nava, F. et al. *IEEE Trans. Nuc. Sci.* **NS-26**, 308 (1979).

[58] Alig, R. C., Bloom, S., and Struck, C. W. *Phys. Rev. B* **22**, 5565 (1980).

[59] Alig, R. C. *Phys. Rev. B* **27**, 968 (1983).

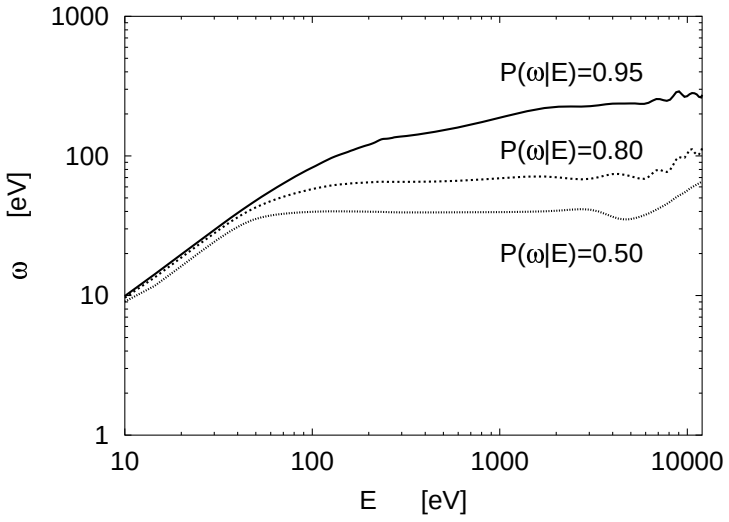

Figure 1: Energy loss, ω, in a single inelastic scattering event during electron-atom interactions in diamond as a function of electron energy. Plots show results at fixed integrated probabilities, $P(\omega|E) = 0.5, 0.8, 0.95$, obtained with the TPP-2 model. The probability $P(\omega|E)$ is the integrated probability that the energy loss in a scattering event is less than or equal ω.

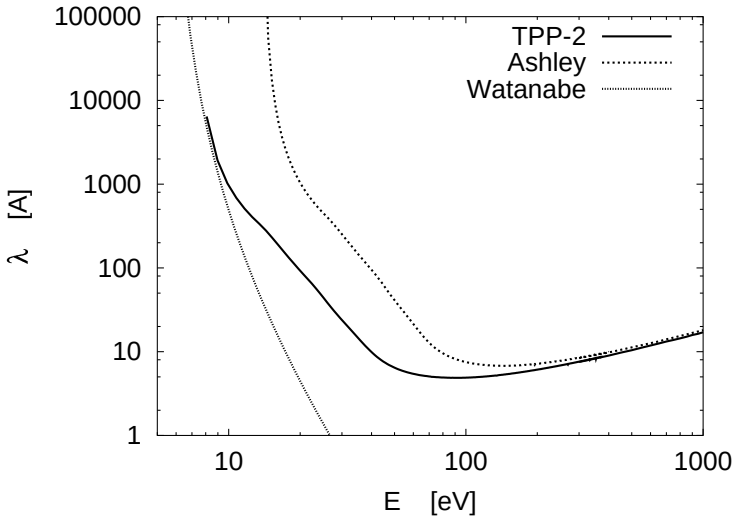

Figure 2: Inelastic mean free paths in diamond obtained with different models: (i) the TPP-2 optical model (solid line), (ii) Ashley's optical model (dashed line), (iii) first-principles calculations of Watanabe et al. (dotted line).

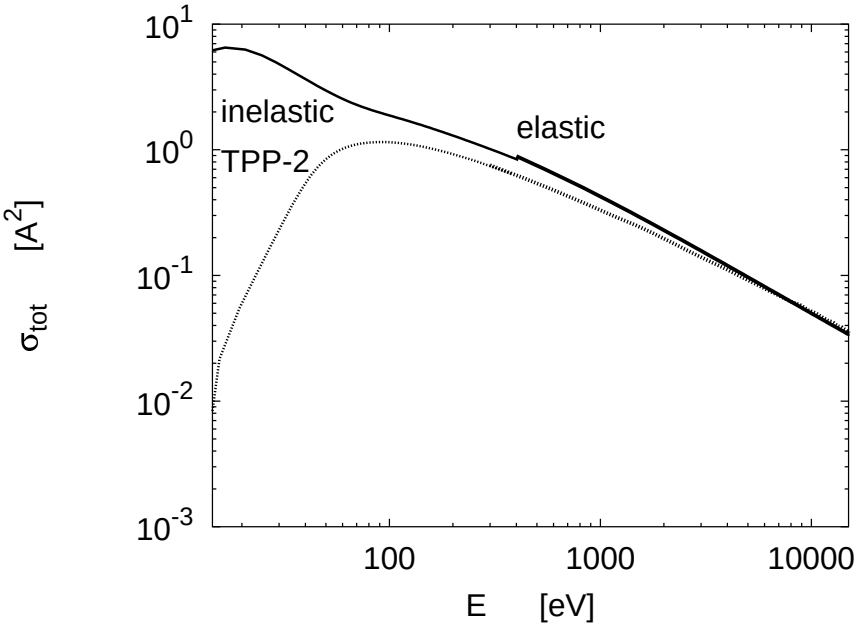

Figure 3: Elastic and inelastic total cross sections for diamond. Inelastic cross sections are obtained from the Lindhard approximation with core ionization taken into account using the TPP-2 optical model. Elastic cross sections (up to energies, $E = 0.4$ keV) were derived with the Barbieri/Van Hove Phase Shift package [44]. For larger energies, the elastic cross sections were taken from the NIST database.

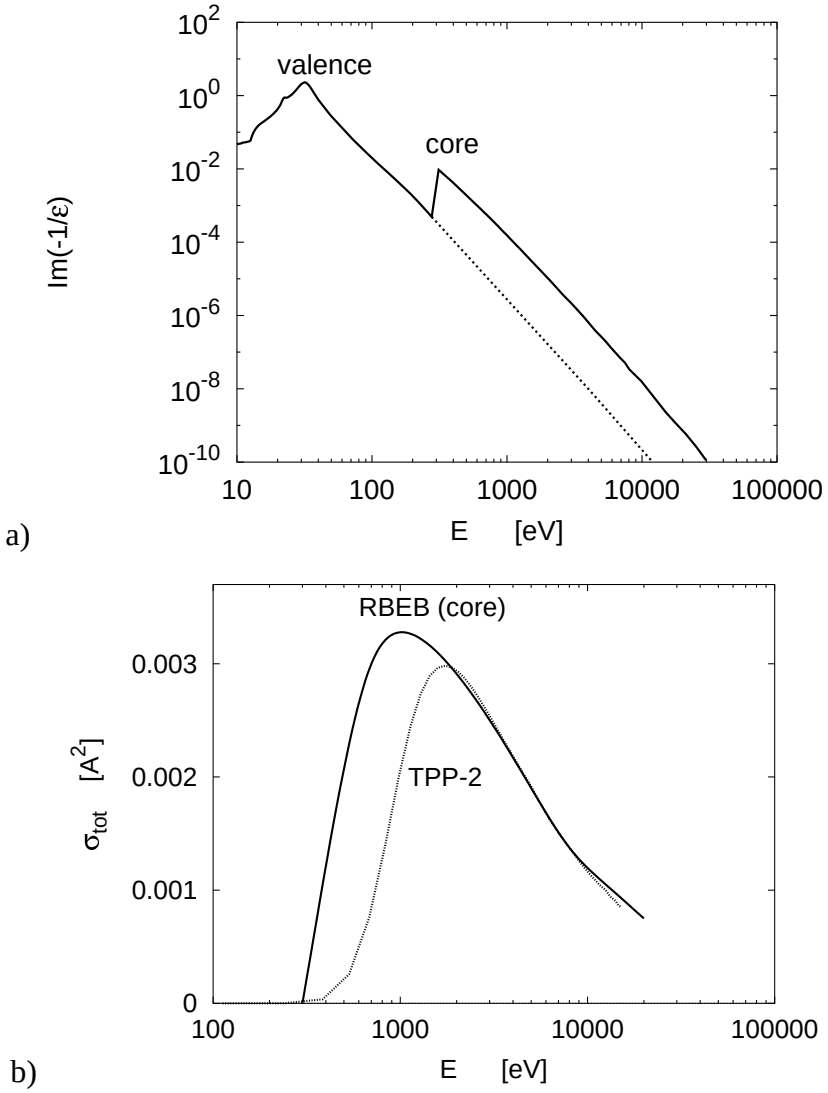

Figure 4: (a) Energy loss function of diamond, $Im(-1/\epsilon)$, (experimental results) and (b) the total cross section for core ionization in diamond. In (b) results from the Lindhard approximation, obtained with the TPP-2 model are compared to the prediction of RBEB model for core ionization from K shell in carbon [46]. The binding energy of a K shell electron in carbon is, $E_B \sim 285$ eV.

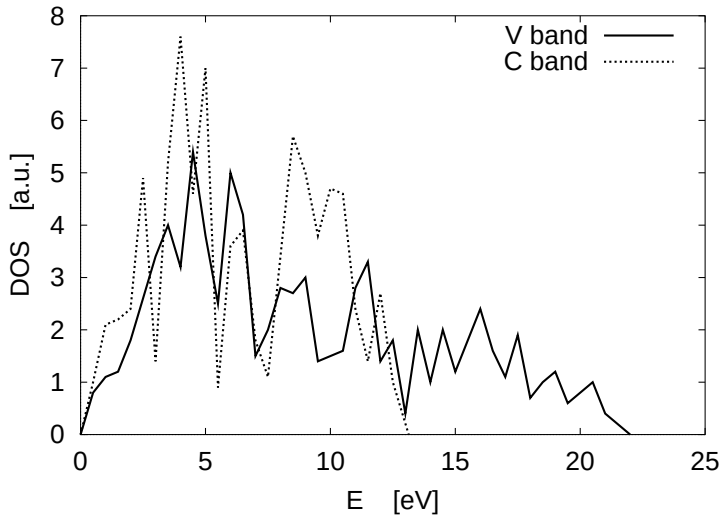

Figure 5: Electronic density of states (DOS) from the calculations by Barnard, Russo and Snook [52]. The calculation was performed with the density functional theory, using CRYSTAL98 package. The density of states of the valence band (solid line) and the density of states of the conduction band (dashed line) were obtained, and the width of bands was estimated to (i) 21.72 eV for the valence band, (ii) 13.13 eV for the conduction band .

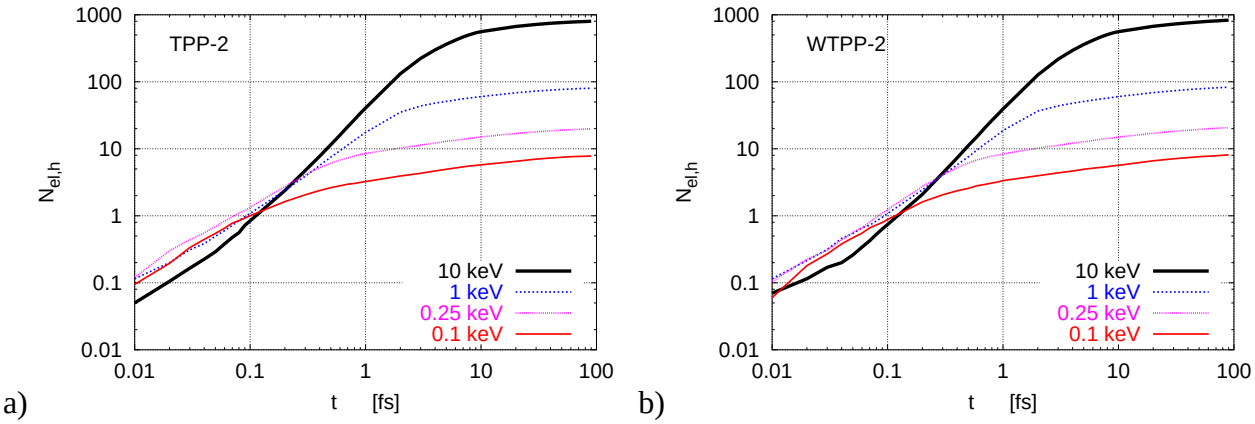

Figure 6: Average number of secondary electrons or holes emitted, $N_{el} = N_h$, vs. time. Curves correspond to the results obtained at different electron impact energies $E = 0.1 - 10$ keV with **(a)** the TPP-2 model, **(b)** the WTPP-2 model.

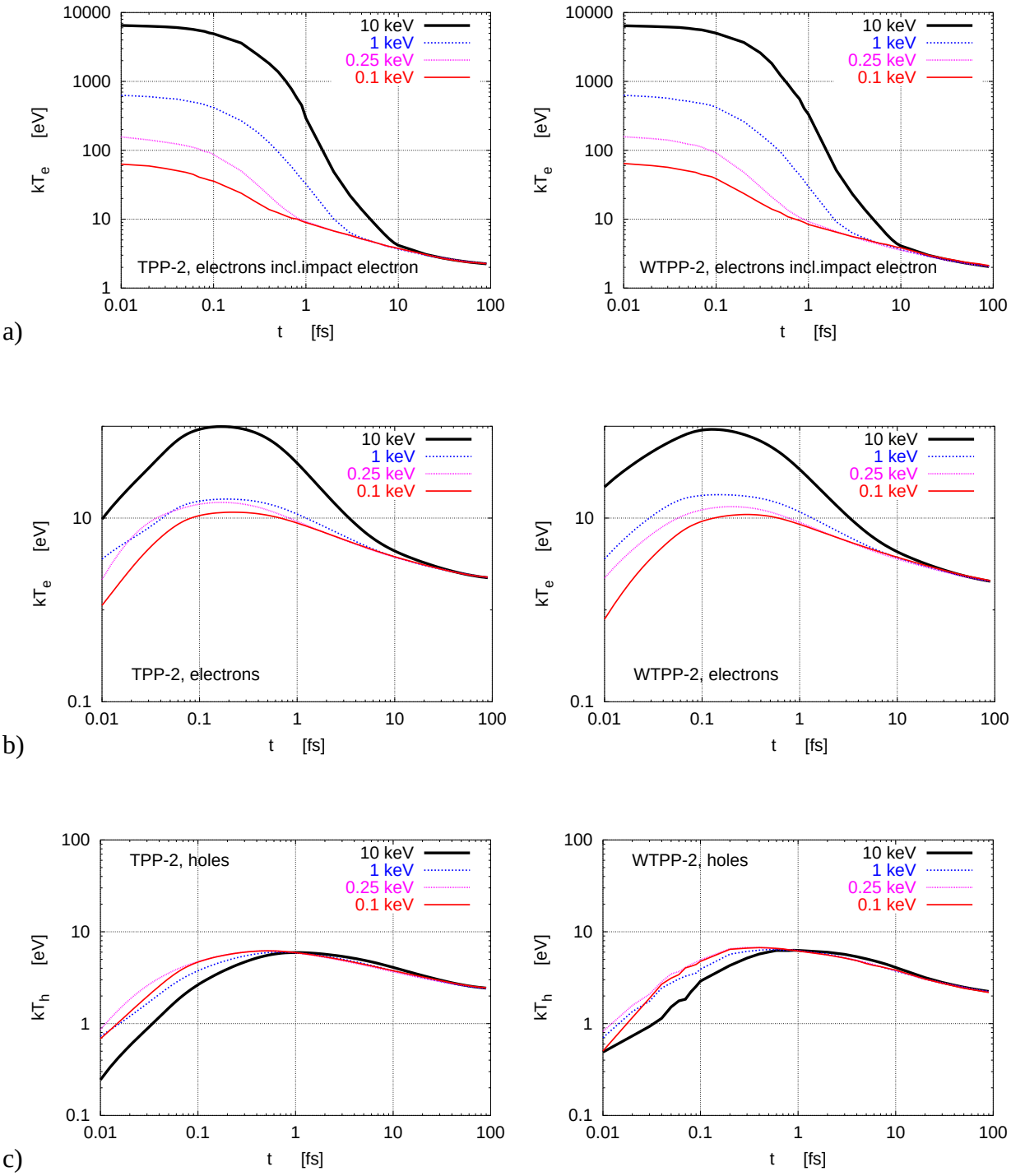

Figure 7: **(a-c)** The equivalent instantaneous temperature kT of carrier gas vs. time averaged over 200 cascades. The temperature was calculated for **(a)** all electrons including the primary electron, **(b)** secondary electrons only, and **(c)** holes. Curves correspond to the results obtained at different electron impact energies $E = 0.1 - 10$ keV from the TPP-2 model (left) and the WTPP-2 model (right).

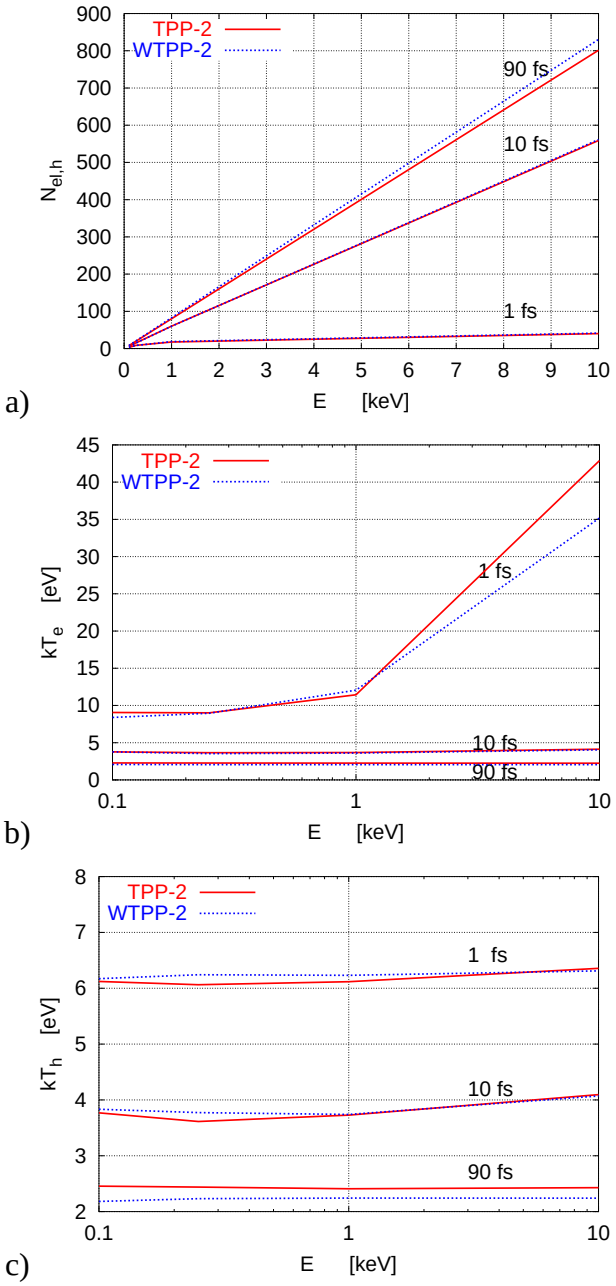

Figure 8: **(a)** Average number of secondary electrons or holes emitted, $N_{el} = N_h$, is plotted vs. energy, E; **(b-c)** The equivalent instantaneous temperature kT of the carrier gas, averaged over 200 cascades is plotted vs. energy, E. Curves correspond to the results obtained for: (b) secondary electrons, and (c) holes at different times $t = 1, 10, 90$ fs from the TPP-2 model (solid line) and the WTPP-2 model (dashed line). The data in (a), (b), and (c) were sampled at primary energies of $E = 0.1, 0.25, 1, 10$ keV.

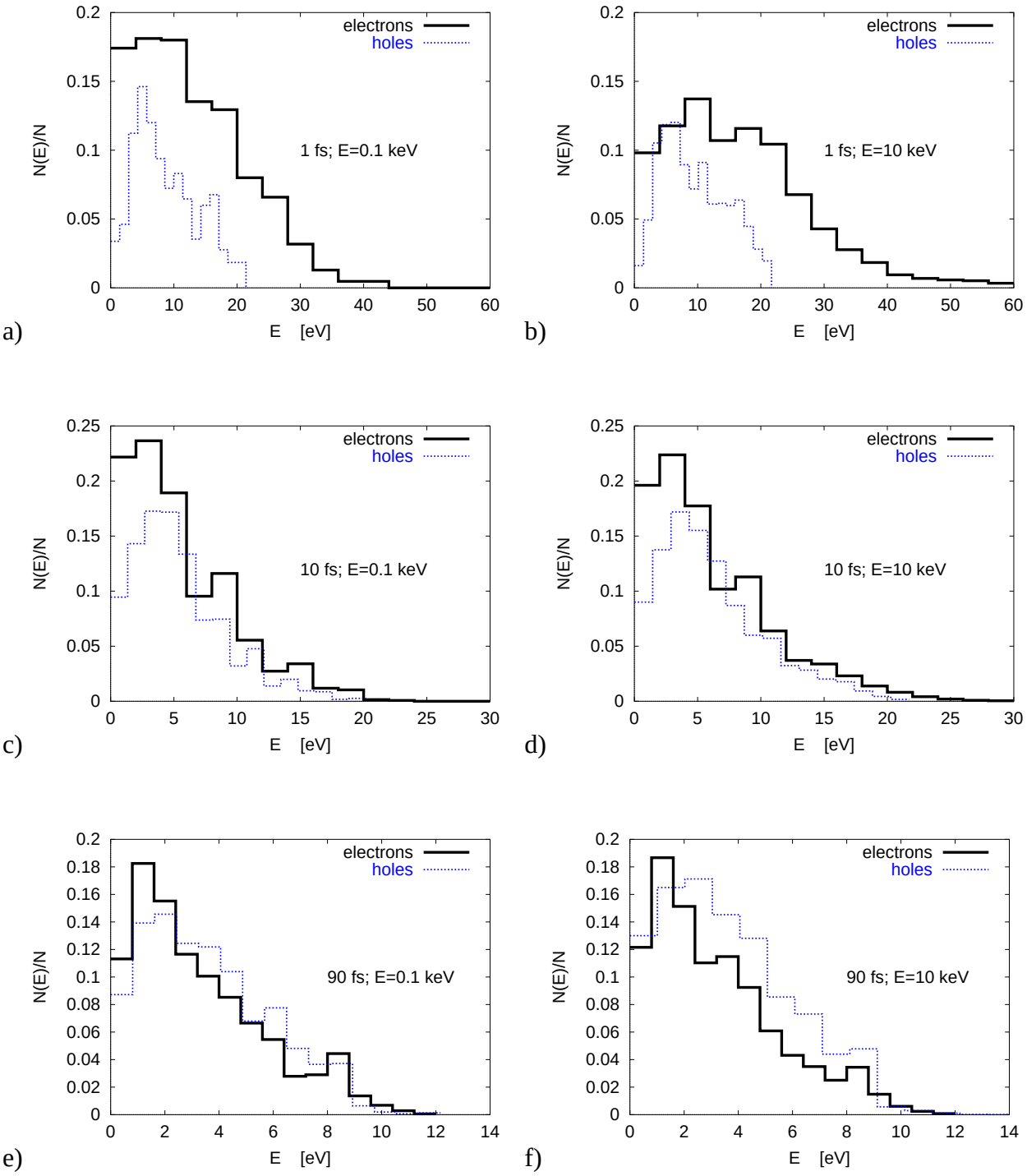

Figure 9: Energy distribution, $N(E)/N$, (fraction of carriers per bin) among carriers (histogram) at **(a-b)** $t = 1$ fs; **(c-d)** $t = 10$ fs; and **(e-f)** $t = 90$ fs. Histograms correspond to results obtained at electron impact of $E = 0.1$ keV (left) and $E = 10$ keV (right) from the TPP-2 model for electrons and holes. The results are plotted for both electrons (solid line) and holes (dashed line).

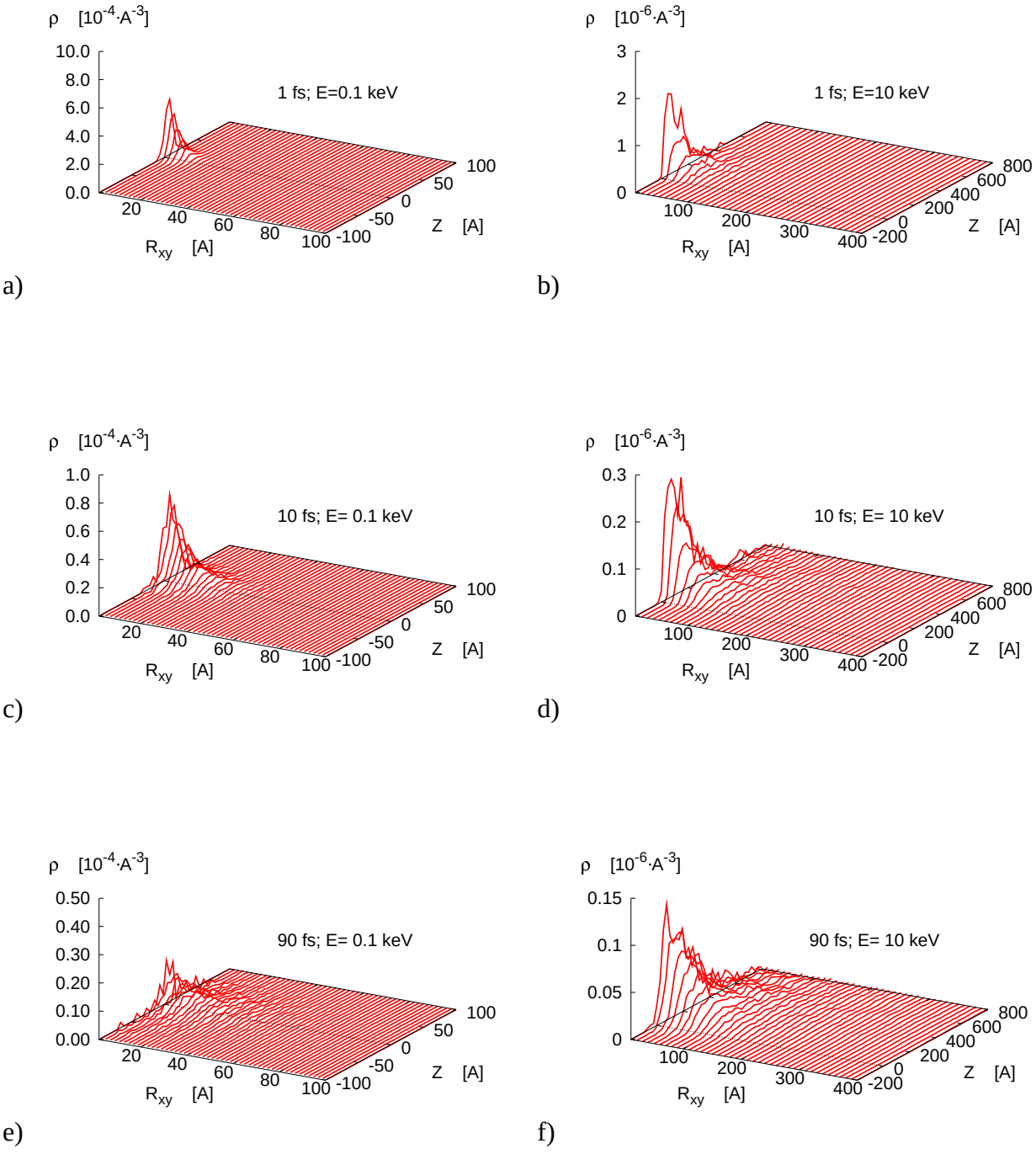

Figure 10: Local electron density estimated for the electron cloud. The data were collected at times: **(a-b)** $t = 1$ fs, **(c-d)** $t = 10$ fs, **(e-f)** $t = 90$ fs at primary energies of $E = 0.1$ keV (left) and 10 keV (right) with the TPP-2 model. The data from the WTPP-2 model are similar (not shown).